

Contents lists available at ScienceDirect

Polymer

journal homepage: www.elsevier.com/locate/polymer





Heat capacity and index of refraction of polyzwitterions

Andrew Clark a, Michael Rosenbaum , Yajnaseni Biswas b, Ayse Asatekin b, Peggy Cebe a,*

- a Department of Physics and Astronomy, Tufts University, Medford, MA, USA
- b Department of Chemical and Biological Engineering, Tufts University, Medford, MA, USA

ABSTRACT

Specific heat capacities and indices of refraction were measured for a series of six sulfobetaine zwitterionic polymers and compared to topological and group contribution models. Poly(sulfobetaine methacrylate) (PSBMA), poly(sulfobetaine acrylate) (PSBA), poly(ethyl sulfobetaine methacrylate) (PSBMA), poly(sulfobetaine methacrylate) (PSBMAM), poly(sulfobetaine acrylate) (PSBAVP) were specially synthesized with changes of chemical structure in order to study effects of either the polymer backbone or the side group on their properties. Temperature modulated differential scanning calorimetry (TMDSC) as well as quasi-isothermal TMDSC were used to determine the temperature dependent specific heat capacity, $c_p(T)$ from 30 to 200 °C. The solid state specific heat capacities were measured for all the polyzwitterions, while liquid state heat capacity measurements were limited to PSBA and PESBMA. Ellipsometry at wavelengths from 300 nm to 3000 nm was used to measure the index of refraction for polyzwitterion thin films at room temperature. Theoretical room temperature values of c_p and n were calculated for the polyzwitterions using topological and group contribution methods and compared to the measured values. The measured index of refraction values agree well with predictions for the polyzwitterions. However, for the solid state heat capacity, the model produces accurate prediction only for PSB2VP and PSB4VP. The discrepancy between the measured and predicted c_p values is most likely due to the reduction of vibrational degrees of motion in the solid state for some of the polyzwitterions due to physical crosslinking.

1. Introduction

Polyzwitterions (PZIs) are polymers that have a side group that contains a covalently linked anion and cation [1]. Polyzwitterions are useful in a number of applications due to their unique electronic structure. They are highly biocompatible since the zwitterionic side groups mimic the structure of a phospholipid head group allowing them to be used as wound dressing material and for drug delivery [2–4]. When used in filtration applications, the zwitterionic structures provide antifouling properties to filtration membranes [5,6]. Polyzwitterions are also capable of dissolving molar ratios of salts, which makes them an ideal polymer to use in solid polymer electrolytes [7–10].

The zwitterionic side groups of polyzwitterions can also interact through dipole-dipole interactions either within the same polymer chain (intrachain) or with neighboring chains (interchain) [1,10,11]. These dipole-dipole interactions result in fully amorphous polymers that exhibit no long-range molecular ordering. The interactions also serve as physical crosslinks that stabilize the polymer and impart improved mechanical strength, making PZIs excellent polymers to use in hydrogel applications [12–14]. The stabilization from these physical crosslinks typically results in exceptionally high glass transition temperatures for polyzwitterions [15–17]. In fact, due to the presence of physical crosslinks, many PZIs do not express their glass transition relaxation process

before the onset of thermal degradation when heating at the slow rates of conventional scanning calorimetry [15,16,18]. Using fast scanning calorimetry, our group reported the glass transition temperatures of several new PZIs [17].

Studies investigating the solution properties of polyzwitterions find that the formation of the physical cross links is thermo-reversible, and there seems to be some evidence of thermo-reversibility in hydrogel systems composed of PZIs [19-21]. However, no study of dry polyzwitterions (i.e., those free of bound water) has shown conclusively that the formation of the crosslinks is thermo-reversible. Furthermore, there have been relatively few in-depth studies of the thermal properties of dry polyzwitterions. One study by Galin et al. performed thermal analysis on five polyzwitterions, and found that only one of their polyzwitterions displayed a glass transition prior to thermal degradation [15]. Cardoso et al. used differential scanning calorimetry (DSC) to measure the glass transition of a polyzwitterion with an exceptionally long side group which lowered the glass transition sufficiently to allow for calorimetric measurement of T_g [22]. To our knowledge, no studies report on either the solid or the liquid state specific heat capacities of polyzwitterions. The specific heat capacity is a fundamental characteristic of a material and measurement of cp can deepen our understanding of both the influence of structure on a material's properties and the structural relaxations associated with the glass transition [23-25].

E-mail address: peggy.cebe@tufts.edu (P. Cebe).

 $^{^{\}ast}$ Corresponding author.

Precise quantification of the specific heat capacity of polyzwitterions can offer insight into the stabilization and constraints introduced into the material by the physical crosslinks. Similar to the heat capacity, the index of refraction of a material is intimately linked to its chemical structure as well as the presence of crystals or other confined phases [26–28]. Formation of physical crosslinks can result in a change in density of dry polyzwitterions, which would influence the index of refraction. Studies of the optical properties of zwitterionic polymers and copolymers have mainly focused on the influence of solvent uptake, rather than on the influence of the polymer structure on the index of refraction [29–32].

Here we report a systematic investigation of the thermal and optical properties of polyzwitterions (PZIs) using thermal analysis, and spectroscopic ellipsometry, respectively. Thermogravimetry is employed to determine both the amount of bound water among the PZIs as well as identify the appropriate temperature range for measurement of the heat capacity. In order to determine the heat capacity for these systems we use temperature modulated DSC in both standard and quasi-isothermal (QI) mode. TMDSC and QI-TMDSC allow for high precision measurement of the heat capacity without the influence of any non-reversing components. A variable angle spectroscopic ellipsometer is used to measure the index of refraction of the polyzwitterions.

The six PZIs, shown in Fig. 1, are members of the sulfobetaine family of polyzwitterions, and all contain the same sulfobetaine anion. The synthesis of several of these novel PZIs has recently been reported by our group [17]. The structure of the six polymers has been systematically varied from the parent polyzwitterion, poly(sulfobetaine methacrylate) (PSBMA). In particular, poly(sulfobetaine acrylate) (PSBA) has an acrylate backbone rather than a methacrylate backbone, poly(ethyl sulfobetaine methacrylate) (PESBMA) has ethyl groups on the quaternary ammonia as opposed to methyl groups, and poly(sulfobetaine methacrylamide) (PSBMAm) has a methacrylamide group connecting the side group to the backbone as opposed to the methacrylate connector. The last two PZIs poly(sulfobetaine 2-vinylpyridine) (PSB2VP) and poly(sulfobetaine 4-vinylpyridine) (PSB4VP) have the most extreme variation, with the sulfobetaine group connected to the backbone through a pyridine ring. Variations in chemical structure that alter backbone flexibility and side group bulk in conventional polymers has been shown to have pronounced effects on their thermal properties [33,34]. The PZIs shown in Fig. 1 have chemical variations that result in bulkier side groups (PESBMA, PSBMAm, PSB2VP and PSB4VP), as well as more flexible backbones (PSBA, PSB2VP and PSB4VP), which will allow for a thorough investigation of the influence of chemical structure in PZIs.

Index of refraction and heat capacity are two macroscopic properties that directly relate to both the atomic and chemical structure of a material. While they both are directly related to the polymer structure, the means by which they interrogate that structure are different. Any deviation between measured and predicted heat capacity and index of refraction will allow for a more complete understanding of how the different polymer chemistries are impacting the higher order structure. In addition to measuring the heat capacity and index of refraction we use

two methods of predicting the room temperature specific heat capacities and indices of refraction of these polymers a priori from their chemical structures. The two methods developed by Bicerano and by van Krevelen take two different predictive approaches: the Bicerano method uses a topological method to consider the molecular connectivity indices, while the van Krevelen method uses group contribution and additivity methods [27,28]. Both have been successful for predicting the specific heat capacities and indices of refraction for a large number of polymers [27,28,35]. By comparing predictions with our measurements we can gain valuable insight into how the zwitterionic structure influences two important macroscopic properties.

2. Experimental section

2.1. Sample synthesis and fabrication

Sulfobetaine methacrylate (SBMA), sulfobetaine methacrylamide (SBMAm), N, N-dimethyl aminoethyl acrylate (DMAEA), N, N-diethyl aminoethyl methacrylate (DEAEMA), 2-vinylpyridine (2-VP), 4-vinylpyridine (4-VP), 1,3-propanesultone, 2,2,6,6-tetramethylpiperidine 1-oxyl (TEMPO), azobisisobutyronitrile (AIBN), monomethyl ether of hydroquinone (MEHQ) were purchased from Sigma Aldrich. The monomer synthesis and subsequent polymerization of the series of six polyzwitterions shown in Fig. 1 has previously been reported by our group [17].

2.2. Fabrication of films

Bulk polyzwitterions were prepared by first dissolving as-received powders in 2,2,2-trifluoroethanol (TFE, Alfa Aesar) at a concentration of 10% g/mL and mixing at room temperature for at least 1 h. Once fully dissolved, films were cast from solution into PTFE dishes and allowed to dry under a fume hood for several days. Following this initial drying, cast films were stored in a vacuum oven at 25 °C to remove residual TFE and minimize absorption of ambient water. Thin films for ellipsometry were spun cast from solutions onto mechanical grade silicon wafers (0.675 mm thick) at 1500 RPM from 3 wt% TFE solution. Spun cast films were stored in a vacuum oven at 25 °C to remove residual TFE and minimize absorption of ambient water.

2.3. Thermogravimetry

Thermogravimetry (TG) was performed on a TA Instruments Inc. (New Castle, Delaware) Q500 series thermogravimetric analyzer, heating from 30 °C to 1000 °C under $\rm N_2$ purge at 50 mL/min. Sample masses were between 3 and 15 mg. Standard TG was carried out by heating at 2 °C/min and 5 °C/min to determine thermal stability and amount of bound water. The polyzwitterions were scanned in the thermogravimetric analyzer under isothermal conditions that mimicked the conditions of the QI-TMDSC, to check for signs of degradation which might be caused by long holding times used in QI treatments. The samples were heated at 20 °C/min to 160 °C, then held isothermally for 20 min.

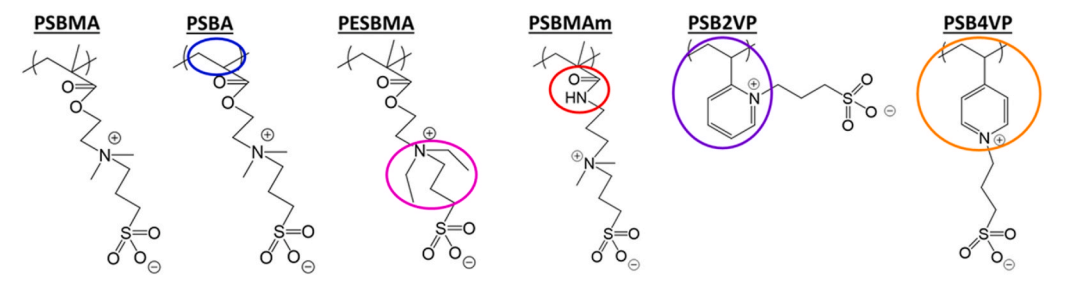


Fig. 1. Chemical structure of the six polyzwitterions investigated in this study. PSBMA is the parent molecule that has been systematically varied to create PSBA, PESBMA, PSBMAm, PSBAVP and PSBAVP. Chemical variations among the PZIs in comparison to PSBMA have been circled for emphasis.

Following the isothermal hold, the temperature was incremented by 2 $^{\circ}$ C and held isothermally again for 20 min. This continued until the samples reached 240 $^{\circ}$ C, after which their heating was continued to 1000 $^{\circ}$ C at 50 $^{\circ}$ C/min.

2.4. Differential scanning calorimetry

Differential scanning calorimetry was performed on a TA Instruments Inc. (New Castle, Delaware) Q100 series DSC equipped with a refrigerated cooling system, and using dry N2 purge at 50 mL/min. The DSC cell was calibrated for temperature and heat flow using an indium standard, and heat capacity using a sapphire standard. Scans were carried out using standard DSC as well as temperature modulated mode (TMDSC). Standard DSC scans were performed at a rate of 10 °C/min on samples with masses between 3 and 10 mg encapsulated in aluminum pans. TMDSC was performed in both standard mode as well as quasiisothermal (QI) mode. TMDSC in standard mode was performed at a rate of 5 °C/min with a modulation period of 60 s and a temperature modulation amplitude of ± 0.796 °C for samples with masses between 3 and 10 mg. Samples were initially heated using DSC at 10 °C/min from 0 °C to 200 °C and held isothermally for 10 min to eject any bound solvent or water and to erase thermal history. Following this step, the samples were cooled to 0 °C and held isothermally for 15 min to ensure steady state conditions. Samples were then heated using TMDSC to 250 °C at 5 °C/min after which they are held isothermally at 250 °C for 15 min to ensure steady state conditions, then subsequently cooled to room temperature.

In order to obtain high-precision specific heat capacity data, a three runs calibration technique was used [36–41]. First an empty aluminum pan was scanned at the given run conditions to provide the baseline correction. A sapphire standard was then scanned to obtain the heat capacity calibration, and finally the polymer sample was scanned. For all three scans the same empty reference pan was used, and its mass was kept to within ± 0.02 mg of the sample pan to minimize any errors due to mass asymmetry [40]. The uncertainty in the heat capacities determined using the three runs method has been shown to range from 1.5% to 3% depending on the specific instrument used [42,43]. For our calorimeter, the heat capacity uncertainty due to instrumental factors is 2.5%. For TMDSC scans, the component of the heat capacity that arises from effects that can be reversed within the period of modulation, known as the reversing heat capacity, is calculated from:

$$\left| mc_p + (C_s - C_r) \pm \Delta C_{cell} \right| = K' \frac{A_{HF}}{A_T} \tag{1}$$

where on the left side c_p is the specific heat capacity of the sample, C_s is the heat capacity of the aluminum pan the polymer is encapsulated in, C_r is the heat capacity of the reference pan, and ΔC_{cell} is the cell asymmetry [36–38]. On the right side, A_{HF} is the amplitude of the heat flow, A_T is the temperature modulation amplitude, and K' is the calibration factor determined from the sapphire reference scan [39,41].

The quasi-isothermal (QI) TMDSC was carried out for all samples with a temperature amplitude of $\pm 0.796~^{\circ}\text{C}$, with an oscillation period of 60 s. Samples were held isothermally for a total of 20 min at each temperature before incrementing to the next temperature. The first 10 min of the isothermal hold was designed to allow the sample to reach steady state conditions and was not used for any subsequent analysis. The second 10-min interval was used for determination of the reversing heat capacity from:

$$mc_p = K' \frac{A_{HF}}{A_T \omega} \tag{2}$$

where ω is the frequency of modulation (defined as $2\pi/P$ where P is the period) while m, c_p , A_{HF} , and A_T are the same as in equation (1) [44]. To assure that steady sate was attained in this second 10-min hold, Lissajous figures of the modulated heat flow as a function of modulated

temperature were examined for overlap of successive cycles (Fig. S1 in the Supplemental Information). For PSBMA, PSBMAm, PSB2VP, and PSB4VP the temperature range for QI TMDSC was from 0 °C to 200 °C, with isothermal holds every 10 °C. For PSBA and PESBMA, multiple samples were used to cover different temperature ranges, to measure the solid-state heat capacity, the T_g region, and the liquid state heat capacity. These measurements ranged from 0 to 240 °C with temperature steps of 2.5 °C, 3 °C, or 10 °C depending on the proximity to a transition region, such as the T_g region.

2.5. Ellipsometry

Ellipsometry was performed on a J.A. Woollam VASETM UV-NIR Spectroscopic Ellipsometer (Lincoln, Nebraska) at 25 °C. Samples were prepared by spin casting polyzwitterion films from a dilute (3 wt/v%) solution onto mechanical grade silicon wafers (Ted Pella Inc., Redding, California). Spin casting allows for the deposition of a thin polymer layer and silicon was chosen as its optical and ellipsometric properties are well known [45]. Cast films were dried in a vacuum oven at 25 °C for a minimum of 24 h prior to ellipsometric scans. The films were stored in a desiccator to ensure minimal uptake of ambient water. The ellipsometric angles Ψ and Δ , were measured at angles near Brewster's angle to maximize the measured signals. For our samples, this angle was found to be near 70° angle of incident light. The scans were recorded over the wavelength range of 300 nm-3000 nm, with a step scan interval of 10 nm. From Ψ and Δ , the film thickness as well as dynamic and equilibrium optical properties such as index of refraction, and extinction coefficient can be extracted using an appropriate physical model [46–48]. We model our system as a two-layer system with the polymer deposited atop the silicon. Both the silicon and polymer layers were assumed to possess uniform thickness.

3. Results and discussion

3.1. Water content and thermal stability of PZIs

Polyzwitterions are hygroscopic and readily absorb water from their environment [1,16,49,50]. The cast polyzwitterion films were stored in a vacuum oven at 25 °C to remove any weakly bound water and to prevent the re-absorption of water [50]. Accurate and precise measurement of the polyzwitterion specific heat capacity is dependent on knowing the mass of the polyzwitterion without the presence of bound water. In order to accurately measure the mass of the PZIs, the amount of water absorbed must be known. We use thermogravimetry to measure both the amount of absorbed water and the thermal degradation temperature of the PZIs. The thermogravimetric scans at 5 $^{\circ}$ C/min are shown in Fig. 2a and b.

Fig. 2a shows the percent of mass remaining for PZIs as a function of temperature from 30 to 600 °C. An initial mass loss step is seen starting from 30 °C that ends around 200 °C, followed by a large mass loss from degradation beginning around 250 °C. The mass remaining after degradation plateaus at different temperatures for different PZIs, and degradation is substantially completed by 450 °C. As temperature further increases to 600 °C, the mass remaining does not drop to zero. The PZIs have between 5% and 40% mass remaining due to degraded polymer char that sticks to the bottom of the TGA basket and is not removed under $\rm N_2$ purge. The methacrylate based polyzwitterions have less char stuck to the pan indicating that they degrade more completely than the polyzwitterions with aromatic side groups.

Fig. 2b shows a magnified view of the first mass loss step, which is caused by loss of bound water. The mass of bound water is determined by finding the height of the step change between 30 $^{\circ}$ C and 200 $^{\circ}$ C. As reported in Table 1, the amount of bound water varies from \sim 1 to 3% for the PZIs without aromatic structure and varies from \sim 11 to 13.5% for the two PZIs containing an aromatic ring, *viz.*, PSB2VP and PSB4VP.

Addition of the aromatic pyridine, and the reduction in aliphatic

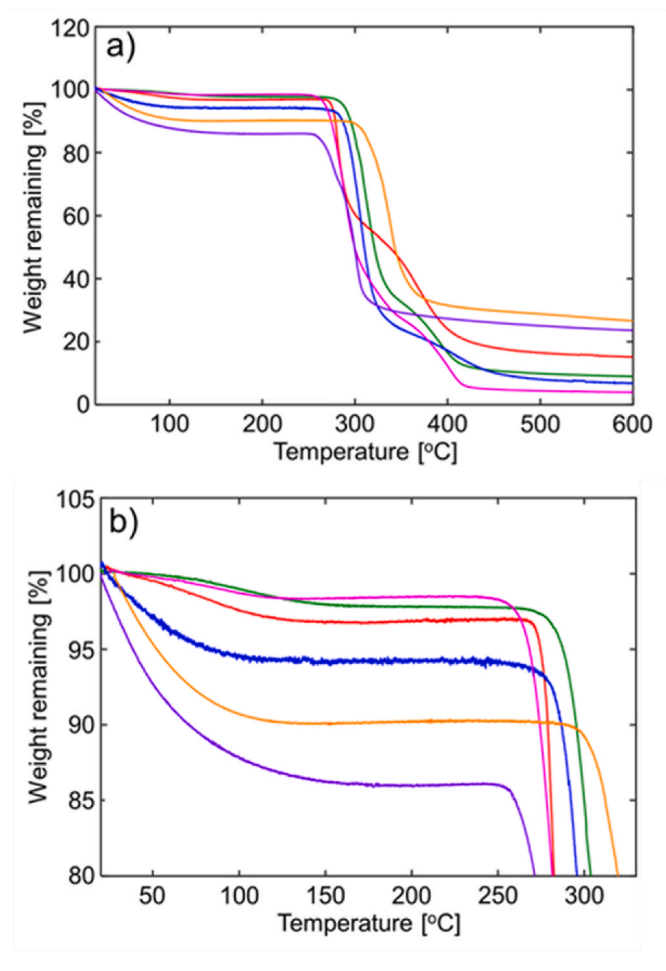


Fig. 2. Thermogravimetric scans of the polyzwitterions at a heating rate of 5 $^{\circ}$ C/min a) Full scale, 30 $^{\circ}$ C-600 $^{\circ}$ C; b) Expanded scale of region from 30 $^{\circ}$ C to 300 $^{\circ}$ C. PZIs are color coded as follows: PSBMA - green, PSBA - blue, PESBMA - magenta, PSBMAm - red, PSB2VP - purple, PSB4VP - orange. (For interpretation of the references to color in this figure legend, the reader is referred to the Web version of this article.)

linkers in the zwitterionic side group, significantly increase the hydrophilicity of the polyzwitterion. For the methacrylate based PZIs, we see that PSBMA and PESBMA have the smallest amount of absorbed water, while PSBA and PSBMAm have the largest amount of absorbed water. The methacrylate backbones of PSBMA and PESBMA are more hydrophobic than either the acrylate backbone of PSBA or the methacrylamide backbone of PSBMAm, resulting in the smaller amount of water absorption in PSBMA and PESBMA. Similarly, the ethyl groups on the quaternary ammonia in PESBMA are more hydrophobic than the methyl group present in PSBMA, leading to smaller amount of absorbed water in PESBMA compared to PSBMA.

Bound water is fully removed in all the polyzwitterions around 200 $^{\circ}\text{C},$ and there is no mass lost to degradation until temperature

increases above 250 °C as seen in Fig. 2b. As shown in Table 1, PESBMA shows the lowest thermal stability with degradation onset at 265 °C, while the other five PZIs show degradation onset temperatures $10\text{--}40\,^{\circ}\text{C}$ higher. All six PZIs show a multi-step degradation profile which has been observed in other zwitterionic systems [6,50–53]. We use the onset of thermal degradation from these TG studies to set the upper limit for any DSC measurements, so as to avoid thermal degradation while measuring heat capacity. From the TG results, we choose 250 °C as the ultimate upper temperature limit to maximize the temperature range measured while minimizing thermal degradation for the non-isothermal standard and modulated DSC experiments.

Following previous work by our group, we utilize a combination of TMDSC, and quasi-isothermal TMDSC (QI-TMDSC) to measure the heat capacity of these PZIs [36,38,39]. QI-TMDSC measurements involve long isothermal holds, which increases the risk of thermal degradation in the PZIs during the scan. To assess this risk we first performed a "pseudo-QI" scan using thermogravimetry. The samples were placed in the thermogravimetric analyzer and heated to 160 °C at 20 °C/min and then held isothermally for 20 min. Following this hold, the temperature was increased by 2 °C and the sample was again held isothermally for 20 min. This procedure was iterated until the sample reached 240 °C. This procedure mimics the isothermal holds of the QI-TMDSC measurement and results are shown in Fig. 3. Two degradation steps can be seen in most PZIs, with PSB4VP being the exception. The degradation onset temperature, TD, during pseudo-QI conditions shifted to much lower temperatures for PSBMA, PSBA, PESBMA, PSBMAm, and PSB2VP than the degradation temperature seen during scanning at 5 °C/min. The degradation temperatures found during pseudo-QI testing are shown in the second row of Table 1. Longer times spent at high temperature will promote early onset of degradation. In light of the reduced degradation onset temperatures during the long isothermal holds, we set an initial upper limit temperature of 200 °C for the quasi-isothermal DSC when measuring the specific heat capacity provided no glass transition was expressed. The upper temperature limit was increased in cases where a glass transition was observed above 200 °C in TMDSC.

3.2. Specific heat capacity of PZIs

Results of temperature modulated differential scanning calorimetry are shown in Fig. 4. In Fig. 4a-b the total, reversing and non-reversing heat flow rate for PSBA and PESBMA are shown as functions of temperature, with curves vertically shifted for clarity. A step change around 200 °C is observed in both the total and reversing heat flow rate for both PSBA and PESBMA, indicative of the glass transition process. In the total and non-reversing heat flow rates we also observe a small endotherm in the same temperature region. This endotherm, called "enthalpy relaxation", arises from the physical relaxation of the polymer caused by the 15-min isothermal hold at 0 $^{\circ}$ C, a common feature seen in the glass transitions of fully amorphous polymers [38,54,55]. In our previous study utilizing fast scanning calorimetry, the glass transition temperatures for PSBA and PESBMA were measured to be 196 °C and 186 °C, respectively, using Moynihan's method [17]. The T_g values we observe here agree with the values measured in FSC, which is further indication that no degradation has occurred in our samples. The presence of the

 Table 1

 Polyzwitterion degradation onset temperature and bound water content.

Polymer	PSBMA	PSBA	PESBMA	PSBMAm	PSB2VP	PSB4VP
Degradation Onset [°C]a	296 ± 1	290 ± 1	276 ± 1	265 ± 1	265 ± 1	304 ± 1
Degradation Onset [°C] ^b	228 ± 1	226 ± 1	225 ± 1	235 ± 1	218 ± 1	-
Bound Water TGA [%] ^c	1.66 ± 0.33	3.38 ± 1.57	1.44 ± 0.20	2.08 ± 0.67	13.16 ± 0.58	12.81 ± 1.56

Data unavailable for this sample.

^a Degradation onset for standard TG at 5 °C/min.

^b Degradation onset for pseudo-QI TG.

^c Uncertainty determined from multiple TG scans.

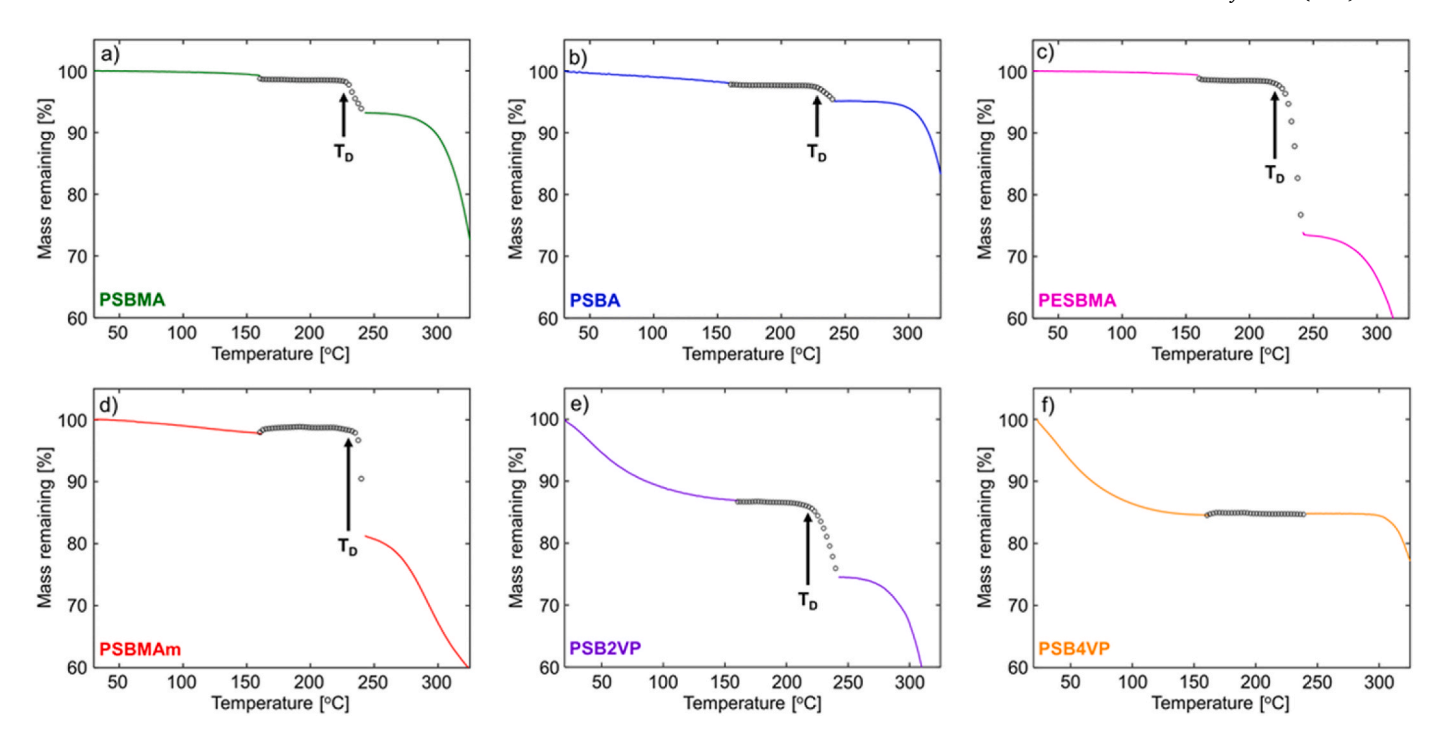


Fig. 3. Combination thermogravimetric scans of polyzwitterions showing heating at 20 °C/min (solid curve below 160 °C), pseudo-QI conditions with 20-min isothermal holds (black circles), and final heating at 50 °C/min (solid curve above 230 °C) for: a) PSBMA; b) PSBA; c) PESBMA; d) PSBMAm; e) PSB2VP; and, f) PSB4VP.

glass transition in these two polymers allows quantification of both the solid state and (over a limited temperature range) the liquid state heat capacities. The reversing heat flow rates for PSBMA, PSBMAm, PSB2VP, and PSB4VP are plotted in Fig. 4c, with the curves vertically shifted for clarity. The reversing heat flow rate varies linearly with temperature for these four polyzwitterions and, unlike PSBA and PESBMA, these PZIs show no glass transition over the temperature range we examined. PZIs tend to have exceptionally high glass transition temperatures due to the formation of intra- and interchain physical crosslinks resulting from the zwitterion dipole-dipole interactions [15,22,56]. In particular, PZIs with shorter side group lengths frequently degrade before showing a glass transition in calorimetric scans at conventional heating rates [15,18,57]. For PSBMA, PSBMAm, PSB2VP, and PSB4VP no glass transition is seen prior to the onset of degradation.

The measured specific heat capacities are shown for PSBA in Fig. 5a–b, and for the other five PZIs in Figs. S3a–e of the Supplemental Information. We plot the total heat capacity (dashed back line) in addition to the reversing specific heat capacity from TMDSC (solid blue line), and the reversing specific heat capacity measured using QI-TMDSC (blue and red circles). Away from the glass transition region, all three measured heat capacities overlap well in the solid state. Above $T_{\rm g}$ in the liquid state there is good overlap until around 235 °C, at which point, the QI sample (red circles) starts to thermally degrade. In the glass transition region, the total specific heat capacity deviates from the TMDSC and QI-TMDSC reversing specific heat capacities due to the presence of the relaxation endotherm. The QI-TMDSC deviates slightly from the standard TMDSC between 190 °C and 215 °C, most likely due to the polymer reaching an equilibrium state during the long isothermal hold.

The specific heat capacity is linear for PSBA from 20 °C up to ~ 170 °C, which is consistent with the behavior of the solid state heat capacity of polymers above 100 K (-173.15 °C) [28,37]. We also observe a linear temperature dependence of the liquid state heat capacity as suggested by Wunderlich [37]. Multiple polymer samples were used to obtain the liquid state heat capacity using QI-TMDSC, as shown in Fig. 5b. This was done to minimize degradation from the long

isothermal holds. To obtain these data, the samples were heated as fast as possible to above T_g and then the QI protocol was initiated. Using multiple fresh samples, we see that PSBA withstands about five 20 min holds at high temperatures between 220 and 235 before thermal degradation begins at around 235 °C (red open circles). Therefore, when extrapolating the liquid state heat capacity of PSBA, we only consider the QI-TMDSC measurements from 220 °C to 233 °C. For the total and reversing heat capacity, we can measure the liquid state heat capacity up to 250 °C and 240 °C, respectively, due to the greater range of thermal stability

The solid and liquid state specific heat capacities were fitted to linear relationships for all six polyzwitterions and are given in Table 2. The uncertainties in the slope and intercept of the fits were determined by assuming an uncertainty in the measured heat capacities of 2.5% and then using the χ^2+1 method [58]. These relations are determined by averaging the total, reversing and QI determined specific heat capacities in the solid state below T_g , and in the liquid state above T_g . We see that all six PZIs have specific heat capacities with similar slopes in the solid state, arising from their similar chemical structures. In particular, PSB2VP and PSB4VP, which vary only in the position of the nitrogen, have almost identical solid state heat capacities. To the best of our knowledge this is the first measurement of the solid state heat capacity of any polyzwitterion.

3.3. Ellipsometric measurement of index of refraction

Fig. 6a shows the ellipsometric constant, Ψ , of PSB4VP as a function of wavelength, with the proposed two-layer physical model included as an inset. Between 2700 nm and 3000 nm there is a slight dip which is indicative of light being absorbed by the sample. The likely origin of this dip is absorption due to the water in the sample; indeed, this spectroscopic region includes the vibrational band of the –OH group present in water [59]. Despite the absorption of some water, over the course of several ellipsometric scans, the samples showed no significant change in the measured Ψ . Thus, the ellipsometric data represent the equilibrium state of the material comprising PZI and some bound water. The amount

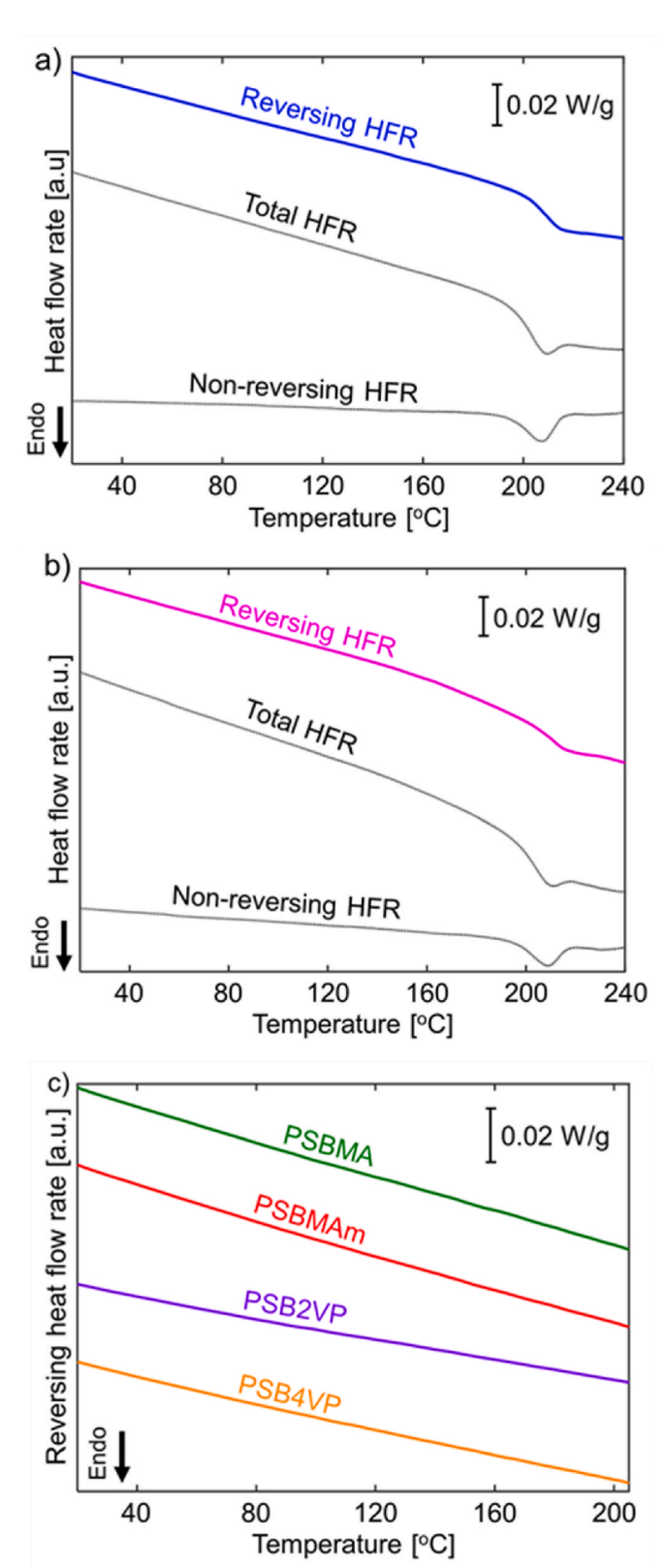


Fig. 4. TMDSC curves as a function of temperature during the second heating with endotherms deflected downwards. The reversing, total, and non-reversing heat flow rates are shown for: (a) PSBA, and (b) PESBMA (curves are shifted vertically for clarity). T_g appears as the step change around 200 °C in the total and reversing heat flow rates, while the relaxation endotherm appears in the total and non-reversing heat flow rates. In (c) the reversing heat flow rates are shown for the remaining polyzwitterions where no T_g is observed (curves have been vertically shifted for clarity).

of absorbed water was not directly measured for the ellipsometric thin film samples. However, it is likely that the amount of absorbed water is comparable to the water content determined by TGA and listed in Table 1.

Two interference fringes are visible as the peaks at 360 nm and 1000 nm, followed by a smooth decrease of Ψ continuing to 2700 nm. Using VASETM software, we fit the ellipsometric data in Fig. 6a to the two-layer model shown in the inset while allowing the thickness of the polymer film to be a fit parameter. The thicknesses of our spun cast films varied between 180 nm and 300 nm. The index of refraction was assumed to be a two term Cauchy function given by Refs. [60,61]:

$$n(\lambda) = A + \frac{B}{\lambda^2} \tag{3}$$

where A and B are fit parameters. The fit to the proposed model is shown in Fig. 6a as the solid black line and shows excellent agreement with the measured data. The index of refraction of PSB4VP is plotted in Fig. 6b. We report the value of n at 589 nm in Table S1 for all six polyzwitterions and the plots of Ψ and $n(\lambda)$ for the other PZIs are shown in the Supplemental Information. The PZIs all show indices of refractions that are consistent with measured values of conventional polymers [27,28].

In the following section, we present a comparison between the experimentally measured indices of refraction and specific heat capacities, and predictions of those quantities. The predictions are based on either topological considerations of the polymer structure, or on chemical group contributions, and have been successful in predicting n and c_p for a wide range of polymers [27,28].

3.4. Comparison between predicted and experimental polyzwitterion heat capacity and index of refraction

Predicting polymer properties has been done by correlating a polymer's macroscopic properties to its underlying chemical structure [28, 62-64]. We use two different methods to calculate the solid state (and, where applicable, liquid state) heat capacities and the indices of refraction at 589 nm at room temperature using the methods of Bicerano and van Krevelen [27,28]. Bicerano's method is a topological method that derives a series of atomic and bond connectivity indices that reflect the local electronic environment of the molecule [27]. Bicerano also includes indices that relate to the number of rotatable bonds present in the molecule. These connectivity and rotational indices were correlated to a number of macroscopic physical properties of polymers including the liquid and solid state heat capacities and indices of refraction [27]. The method of van Krevelen assumes that properties of local chemical groups present in the molecule are additive [28]. This group contribution method is dependent on knowledge of the properties of the underlying groups present, such as methylene groups, ethyl groups, etc. Both methods are capable of providing remarkably accurate predictions of polymer properties for many conventional amorphous and semicrystalline polymers [28,35,65]. As mentioned previously, the heat capacity (in particular, the solid state heat capacity) and index of refraction are ideal physical parameters to model from chemical considerations, as they are intimately tied to a material's molecular structure [37,66,67]. We applied both of these approaches to model the room temperature values of heat capacity and index of refraction (at $\lambda = 589$ nm) of PZIs and compare to our measurements [68].

To better visualize the comparison between measured and predicted values, the predicted values at room temperature are plotted vs. the measured values, in Fig. 7a and b, for heat capacity and index of refraction, respectively. The measured and predicted values are also reported in Table S1 of the Supplement Information. The black lines of slope equal to unity in Fig. 7a and b represent a perfect match between the measured and predicted values. For the methacrylate polyzwitterions (PSBMA, PSBA, PESBMA, and PSBMAm), both predictive methods overestimate the room temperature heat capacity in the solid

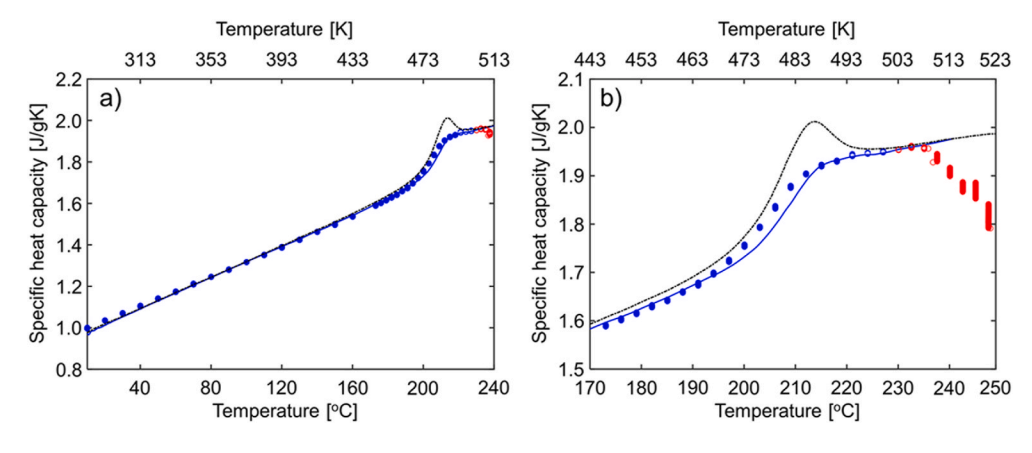


Fig. 5. Specific heat capacity measurements for PSBA. a) A full scale view, from 0 °C to 240 °C. b) An expanded view of the glass transition region from 170 °C to 250 °C. The dashed black line indicates total specific heat capacity, the solid blue line represents the reversing specific heat capacity from standard TMDSC, and the circles represent QI-TMDSC measurements (solid blue circles, open blue circles, and open red circles represent three different polymer samples used to determine the specific heat capacity from QI-TMDSC measurements). (For interpretation of the references to color in this figure legend, the reader is referred to the Web version of this article.)

Table 2Solid and liquid state heat capacities^a for polyzwitterions.

Polymer	c _p ^{Solid.} (T) [J/gK] ^b	c _p ^{Liquid.} (T) [J/gK] †
PSBMA	$(3.66 \pm 0.11) \text{x} 10^{-3} \text{ T} + (0.113 \pm$	-
	0.038)	
PSBA	(3.67 ± 0.12) x 10^{-3} T $ (0.057 \pm$	(1.71 ± 0.93) x 10^{-3} T $+$ $(1.098\pm$
	0.042)	0.479)
PESBMA	(3.99 ± 0.14) x 10^{-3} T $ (0.153 \pm$	$(2.85 \pm 0.50) \mathrm{x} 10^{-3} \mathrm{\ T} + (0.611 \pm$
	0.051)	0.255)
PSBMAm	$(3.66 \pm 0.10) \mathrm{x} 10^{-3} \mathrm{T} + (0.044 \pm$	_
	0.034)	
PSB2VP	(3.62 ± 0.11) x 10^{-3} T + $(0.132 \pm$	_
	0.038)	
PSB4VP	(3.60 ± 0.10) x 10^{-3} T + $(0.120 \pm$	_
	0.039)	

Liquid state data are unavailable due to onset of degradation.

state. For the PZIs containing the pyridine ring (PSB2VP and PSB4VP), both the Bicerano and van Krevelen predictions match the measured heat capacity well as seen in Fig. 7a. The y-axis error bars represent one standard deviation, as given by Bicerano and van Krevelen, suggesting that the deviations seen in the methacrylate polyzwitterion heat capacities are statistically significant and cannot be attributed to statistical fluctuation [27,28].

Different behavior is observed when we compare the predicted and measured indices of refraction for the PZIs. The experimentally measured and predicted indices of refraction are included in Table S1 of the supplement and are graphically represented in Fig. 7b. Again, we observe excellent agreement for PSB2VP and PSB4VP between the measured and predicted values for the index of refraction for both predictive methods. For all the methacrylate polyzwitterions (except PSBMAm) we observe reasonably good agreement between the measured and predicted index of refraction. We can summarize Fig. 7 as follows. Heat capacity and refractive index are well predicted by both methods for PSB2VP and PSB4VP. Both predictive methods produce qualitatively better agreement with the measured refractive indices than with the solid state heat capacity for the methacrylate polyzwitterions. Refractive index of PSBMAm is not predicted well by either method.

The failure of either method to predict the room temperature solid state heat capacity of the methacrylate polyzwitterions most likely arises from formation of physical crosslinks between the zwitterionic side groups. Neither predictive method incorporates crosslink formation in the molecular model. The origin of the solid-state heat capacity lies with the vibrational modes of the polymer [37]. Therefore, formation of inter- and intrachain crosslinks would be expected to result in a

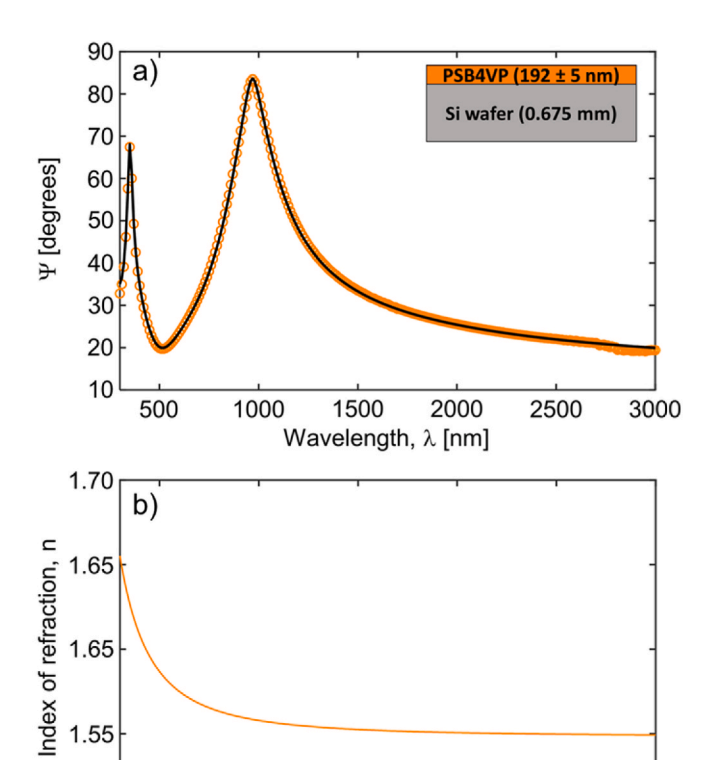


Fig. 6. Ellipsometric data of PSB4VP as a function of wavelength. a) Measured pseudo optical constant Ψ (orange circles), with fitted model (black line). The inset shows a cartoon of the two-layer physical model used fit to the data, comprising a 192 ± 5 nm thick polyzwitterion film on a 0.675 mm thick silicon substrate. Thickness of the polymer film was determined from the fit, while the Si wafer thickness was measured a priori with a micrometer. b) Index of refraction vs. wavelength for PSB4VP returned from fitting to Eqn. (3). (For interpretation of the references to color in this figure legend, the reader is referred to the Web version of this article.)

1500

Wavelength, λ [nm]

2000

2500

3000

disruption of vibrational modes. Van Krevelen notes that from the equipartition theorem, each atom would have thermal energy of $k_B T$ per vibrational degree of freedom, or $3k_B T$. However, in most polymers the presence of neighboring atoms restricts the vibrational degrees of freedom [28]. If we extend this concept to polyzwitterions, then the formation of dipole-dipole physical crosslinks would bring atoms from neighboring side groups into proximity with each other, particularly in the regions near the charge centers, resulting in further reduction of the

1.50

500

1000

 $^{^{\}rm a}$ Linear fits to experimental data from Fig. 5 and S3, with temperature T in Kelvin.

 $^{^{\}text{b}}$ Uncertainty in fit parameters determined using the $\chi^2{+}1$ method as described in [58].

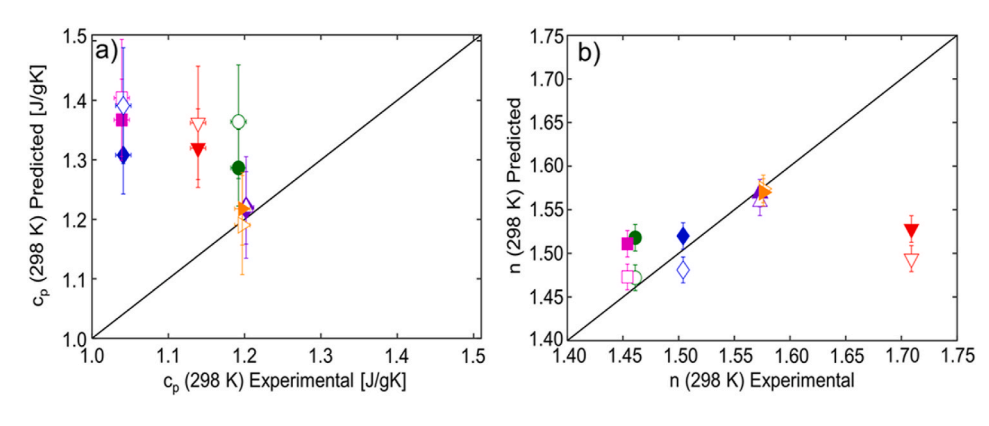


Fig. 7. Comparison of predicted vs. experimentally measured properties of polyzwitterions at room temperature: (a) solid state heat capacity; (b) index of refraction. PSBMA – green circles, PSBA – blue diamonds, PESBMA – magenta squares, PSBMAm – red downward triangles, PSB2VP – purple upward triangles, and PSB4VP – orange right facing triangles. Filled symbols - Bicerano method [27], open symbols - Van Krevelen method [28]. The black lines represent equality between predicted and measured values. (For interpretation of the references to color in this figure legend, the reader is referred to the Web version of this article.)

degrees of freedom per atom. Similarly, a longer side group would allow for a larger number of potential interactions. These reductions in the degrees of freedom in polyzwitterions would invalidate the simple concept of additivity of the group contributions for the solid state heat capacity. Formation of dipole-dipole physical crosslinks influences the local electronic and atomic structures of the molecule, and the connectivity indices defined by Bicerano would also have to change to reflect the reduction in the degrees of freedom of the atoms. The formation of these physical cross-links as well as the overall degree of cross-linking within a polyzwitterion system, would allow for further refinement of these predictive models. Unlike chemical cross-links, however, the physical cross-links formed via dipole-dipole interactions can be reversible, thus making the degree of cross-linking a characteristic that requires direct measurement for each system being tested [17,19,21]. To date no direct measurement method exists that can quantify the degree of physical cross-linking in polyzwitterions and requires further research to develop a robust technique for measuring the degree of physical crosslinking.

We find better agreement between the measured and predicted values of the indices of refraction. The index of refraction depends on both the refractive power of the individual chemical groups, and on the amount of monomer per unit volume. For example, different indices of refraction are measured for the same polymer when its physical state changes from fully amorphous to semicrystalline, due to the increased density of the crystalline phase [27,28]. The polyzwitterions do not have a crystalline form; their fully amorphous nature suggests that their indices of refraction are primarily determined by the polarizability of the underlying chemical groups. Thus, the additivity of group contributions (used by van Krevelen [26]) and the topological approach of bond connectivity indices (as used by Bicerano [27,28]) should be valid in the refractive index models in the case of PZIs. This would also imply that the intra- and inter-chain physical crosslinks which alter the vibrational spectra do not change the density of the polyzwitterions enough to affect the index of refraction for most of the PZIs we investigated. PSBMAm is the only PZI to show significant deviation between the measured and predicted values of the index of refraction. This discrepancy may arise due to the amide connection between the backbone and sidechain, which may result in a larger value of polymer density compared to its predicted density.

4. Conclusions

The heat capacities and indices of refraction of six sulfobetaine type polyzwitterions have been systematically measured. PZIs PSBMA, PSBMAm, PSB2VP and PSB4VP thermally degraded before the onset of the glass transition consistent with the behavior of many PZIs, allowing for measurement of the solid-state heat capacity but not the liquid state. PSBA and PESBMA underwent glass transitions prior to the onset of degradation. For these two PZIs, we were able to measure both the solid state heat capacities and (over a more limited temperature range) their

liquid state heat capacities. The room temperature indices of refraction of the PZIs were also measured using spectroscopic ellipsometry, with the PZIs showing indices of refraction in the typical range seen for conventional polymers. Topological and group contribution methods were used to predict both the room temperature solid-state heat capacities and indices of refraction of the PZIs. The predictions for the methacrylate based PZIs showed overestimations of the measured solid-state heat capacity but good agreement between the measured and predicted indices of refraction. The discrepancy in the heat capacity was attributed to formation of physical crosslinks in the zwitterion that inhibited some of the vibrational modes that contribute to the solid-state heat capacity.

To the best of our knowledge, this work represents the first quantification of the solid and liquid state heat capacities, and indices of refraction, of polyzwitterions. The variation in chemical structure affected the affinity for water, and also resulted in changes in the predicted values for the index of refraction and solid state heat capacity. We find that for PZIs with aromatic structures in the side groups, both the solid state heat capacity and index of refraction are accurately predicted. For PZIs without bulky aromatic structures, the prediction schemes used are less accurate. Knowledge of these fundamental properties will allow for more targeted studies that can help uncover how the unique zwitterionic structure influences macroscopic properties as well as material applications of polyzwitterions.

CRediT authorship contribution statement

Andrew Clark: Investigation, Formal analysis, Writing – original draft, Writing – review & editing. Michael Rosenbaum: Investigation, Formal analysis. Yajnaseni Biswas: Investigation, Resources. Ayşe Asatekin: Conceptualization, Funding acquisition, Supervision, Writing – review & editing. Peggy Cebe: Conceptualization, Funding acquisition, Supervision, Writing – review & editing.

Declaration of competing interest

The authors declare that they have no known competing financial interests or personal relationships that could have appeared to influence the work reported in this paper.

Data availability

Data will be made available on request.

Acknowledgments

Support for this research was provided by a Tufts Collaborates Seed Grant, National Science Foundation, Polymers Program of the Division of Materials Research, under DMR-1608125, DMR-2003629 and through the MRI Program under DMR-0520655 which provided thermal

analysis instrumentation. The authors thank the Polymers for Advanced Technology 2019 interns Mr. Joseph Adjei, Ms. Mikaila Fini, Ms. Amy Johnson, and Ms. Jessica McBeth of Rochester Institute of Technology and National Technical Institute for the Deaf for their contributions in the preliminary analysis and characterization of these polymers. The authors also thank Professor Tom Vandervelde and Dr. Kevin Grossklaus for access and training on use of the J.A. Woolam Vase™ Ellipsometer.

Appendix A. Supplementary data

Supplementary data to this article can be found online at https://doi.org/10.1016/j.polymer.2022.125176.

References

- [1] A. Laschewsky, Structures and synthesis of zwitterionic polymers, Polymers 6 (2014) 1544–1601.
- [2] W. Yang, H. Xue, L.R. Carr, J. Wang, S. Jiang, Zwitterionic poly (carboxybetaine) hydrogels for glucose biosensors in complex media, Biosens. Bioelectron. 26 (2011) 2454–2459
- [3] R. Lalani, L. Liu, Electrospun zwitterionic poly (sulfobetaine methacrylate) for nonadherent, superabsorbent, and antimicrobial wound dressing applications, Biomacromolecules 13 (2012) 1853–1863.
- [4] J.T. Sun, Z.Q. Yu, C.Y. Hong, C.Y. Pan, Biocompatible zwitterionic sulfobetaine copolymer-coated mesoporous silica nanoparticles for temperature-responsive drug release, Macromol. Rapid Commun. 33 (2012) 811–818.
- [5] P. Kaner, E. Rubakh, A. Asatekin, Zwitterion-containing polymer additives for fouling resistant ultrafiltration membranes, J. Membr. Sci. 533 (2017) 141–159.
- [6] N. Govinna, P. Kaner, D. Ceasar, A. Dhungana, C. Moers, K. Son, A. Asatekin, P. Cebe, Electrospun fiber membranes from blends of poly (vinylidene fluoride) with fouling-resistant zwitterionic copolymers, Polym. Int. 68 (2019) 231–239.
- [7] T. Wu, F.L. Beyer, R.H. Brown, R.B. Moore, T.E. Long, Influence of zwitterions on thermomechanical properties and morphology of acrylic copolymers: implications for electroactive applications, Macromolecules 44 (2011) 8056–8063.
- [8] F. Lind, L. Rebollar, P. Bengani-Lutz, A. Asatekin, M.J. Panzer, Zwitterion-containing ionogel electrolytes, Chem. Mater. 28 (2016) 8480–8483.
- [9] A.J. D'Angelo, M.J. Panzer, Decoupling the ionic conductivity and elastic modulus of gel electrolytes: fully zwitterionic copolymer scaffolds in lithium salt/ionic liquid solutions, Adv. Energy Mater. 8 (2018), 1801646.
- [10] L. Rebollar, M.J. Panzer, Zwitterionic copolymer-supported ionogel electrolytes: impacts of varying the zwitterionic group and ionic liquid identities, Chemelectrochem 6 (2019) 2482–2488.
- [11] M.E. Taylor, M.J. Panzer, Fully-zwitterionic polymer-supported ionogel electrolytes featuring a hydrophobic ionic liquid, J. Phys. Chem. B 122 (2018) 8469–8476.
- [12] J. Ning, K. Kubota, G. Li, K. Haraguchi, Characteristics of zwitterionic sulfobetaine acrylamide polymer and the hydrogels prepared by free-radical polymerization and effects of physical and chemical crosslinks on the UCST, React. Funct. Polym. 73 (2013) 969–978.
- [13] J. Ning, G. Li, K. Haraguchi, Synthesis of highly stretchable, mechanically tough, zwitterionic sulfobetaine nanocomposite gels with controlled thermosensitivities, Macromolecules 46 (2013) 5317–5328.
- [14] L. Wang, G. Gao, Y. Zhou, T. Xu, J. Chen, R. Wang, R. Zhang, J. Fu, Tough, adhesive, self-healable, and transparent ionically conductive zwitterionic nanocomposite hydrogels as skin strain sensors, ACS Appl. Mater. Interfaces 11 (2018) 3506–3515.
- [15] M. Galin, E. Marchal, A. Mathis, B. Meurer, Y.M. Soto, J. Galin, Poly (sulphopropylbetaines): 3. Bulk properties, Polymer 28 (1987) 1937–1944.
- [16] P. Köberle, A. Laschewsky, D. Van den Boogaard, Self-organization of hydrophobized polyzwitterions, Polymer 33 (1992) 4029–4039.
- [17] A.G. Clark, Y. Biswas, M.E. Taylor, A. Asatekin, M.J. Panzer, C. Schick, P. Cebe, Glass forming ability of polyzwitterions, Macromolecules (2021). In Press.
- [18] S.A. Rozanski, F. Kremer, P. Köberle, A. Laschewsky, Relaxation and charge transport in mixtures of zwitterionic polymers and inorganic salts, Macromol. Chem. Phys. 196 (1995) 877–890.
- [19] V. Hildebrand, A. Laschewsky, M. Päch, P. Müller-Buschbaum, C.M. Papadakis, Effect of the zwitterion structure on the thermo-responsive behaviour of poly (sulfobetaine methacrylates), Polym. Chem. 8 (2017) 310–322.
- [20] M. Danko, Z. Kroneková, M. Mrlik, J. Osicka, A. bin Yousaf, A. Mihálová, J. Tkac, P. Kasak, Sulfobetaines meet carboxybetaines: modulation of thermo-and ionresponsivity, water structure, mechanical properties, and cell adhesion, Langmuir 35 (2018) 1391–1403.
- [21] R. Schroeder, W. Richtering, I.I. Potemkin, A. Pich, Stimuli-responsive zwitterionic microgels with covalent and ionic crosslinks, Macromolecules 51 (2018) 6707–6716.
- [22] J. Cardoso, O. Soria-Arteche, G. Vázquez, O. Solorza, I. González, Synthesis and characterization of zwitterionic polymers with a flexible lateral chain, J. Phys. Chem. C 114 (2010) 14261–14268.
- [23] P. Cebe, X. Hu, D.L. Kaplan, E. Zhuravlev, A. Wurm, D. Arbeiter, C. Schick, Beating the heat-fast scanning melts silk beta sheet crystals, Sci. Rep. 3 (2013) 1130.

[24] P. Cebe, D. Thomas, J. Merfeld, B.P. Partlow, D.L. Kaplan, R.G. Alamo, A. Wurm, E. Zhuravlev, C. Schick, Heat of fusion of polymer crystals by fast scanning calorimetry, Polymer 126 (2017) 240–247.

- [25] R. Tao, E. Gurung, M.M. Cetin, M.F. Mayer, E.L. Quitevis, S.L. Simon, Fragility of ionic liquids measured by Flash differential scanning calorimetry, Thermochim. Acta 654 (2017) 121–129.
- [26] G.W. Schael, Determination of polyolefin film properties from refractive index measurements, J. Appl. Polym. Sci. 8 (1964) 2717–2722.
- [27] J. Bicerano, Prediction of Polymer Properties, cRc Press, 2002.
- [28] D.W. Van Krevelen, K. Te Nijenhuis, Properties of Polymers: Their Correlation with Chemical Structure; Their Numerical Estimation and Prediction from Additive Group Contributions, Elsevier, 2009.
- [29] Y. Tang, J. Lu, A. Lewis, T. Vick, P. Stratford, Swelling of zwitterionic polymer films characterized by spectroscopic ellipsometry, Macromolecules 34 (2001) 8768–8776.
- [30] K.P.R. Nilsson, J. Rydberg, L. Baltzer, O. Inganäs, Self-assembly of synthetic peptides control conformation and optical properties of a zwitterionic polythiophene derivative, Proc. Natl. Acad. Sci. USA 100 (2003) 10170–10174.
- [31] Z. Sainudeen, P.C. Ray, Nonlinear optical properties of zwitterionic merocyanine aggregates: role of intermolecular interaction and solvent polarity, J. Phys. Chem. 109 (2005) 9095–9103.
- [32] H.-C. Lu, W.-T. Whang, B.-M. Cheng, Switchable structural modification accompanying altered optical properties of a zwitterionic polysquaraine, Chem. Phys. Lett. 500 (2010) 267–271.
- [33] K. Kunal, C.G. Robertson, S. Pawlus, S.F. Hahn, A.P. Sokolov, Role of chemical structure in fragility of polymers: a qualitative picture, Macromolecules 41 (2008) 7232–7238.
- [34] Y.V. Cheban, S.-F. Lau, B. Wunderlich, Analysis of the contribution of skeletal vibrations to the heat capacity of linear macromolecules in the solid state, Colloid Polym. Sci. 260 (1982) 9–19.
- [35] D.C. Rich, P. Cebe, A.K. St Clair, Refractive Indices of Aromatic Polyimides, ACS Publications, 1995.
- [36] H. Xu, P. Cebe, Heat capacity study of isotactic polystyrene: dual reversible crystal melting and relaxation of rigid amorphous fraction, Macromolecules 37 (2004) 2797–2806.
- [37] B. Wunderlich, Thermal Analysis of Polymeric Materials, Springer Science & Business Media, 2005.
- [38] X. Hu, D. Kaplan, P. Cebe, Effect of water on the thermal properties of silk fibroin, Thermochim. Acta 461 (2007) 137–144.
- [39] W. Huang, S. Krishnaji, X. Hu, D. Kaplan, P. Cebe, Heat capacity of spider silk-like block copolymers, Macromolecules 44 (2011) 5299–5309.
- [40] G. Höhne, W.F. Hemminger, H.-J. Flammersheim, Differential Scanning Calorimetry, Springer Science & Business Media, 2013.
- [41] W. Huang, S. Krishnaji, O.R. Tokareva, D. Kaplan, P. Cebe, Influence of water on protein transitions: thermal analysis, Macromolecules 47 (2014) 8098–8106.
- [42] S. Rudtsch, Uncertainty of heat capacity measurements with differential scanning calorimeters, Thermochim. Acta 382 (2002) 17–25.
- [43] C. Schick, Differential scanning calorimetry (DSC) of semicrystalline polymers, Anal. Bioanal. Chem. 395 (2009) 1589.
- [44] H. Chen, P. Cebe, Vitrification and devitrification of rigid amorphous fraction of PET during quasi-isothermal cooling and heating, Macromolecules 42 (2009) 288–292.
- [45] R. Archer, Determination of the properties of films on silicon by the method of ellipsometry, JOSA 52 (1962) 970–977.
- [46] W.-L. Chen, K.R. Shull, T. Papatheodorou, D.A. Styrkas, J.L. Keddie, Equilibrium swelling of hydrophilic polyacrylates in humid environments, Macromolecules 32 (1999) 136–144.
- [47] D. Styrkas, S. Doran, V. Gilchrist, J. Keddie, J. Lu, E. Murphy, R. Sackin, T. Su, A. Tzitzinou, in: R.W. Richards, S.K. Peace (Eds.), Polymer Surfaces and Interfaces III, John Wiley & Sons Ltd., New York, 1999.
- [48] F. Tiberg, J. Brinck, L. Grant, Adsorption and surface-induced self-assembly of surfactants at the solid–aqueous interface, Curr. Opin. Colloid Interface Sci. 4 (1999) 411–419.
- [49] M.G. Santonicola, M. Memesa, A. Meszyńska, Y. Ma, G.J. Vancso, Surface-grafted zwitterionic polymers as platforms for functional supported phospholipid membranes, Soft Matter 8 (2012) 1556–1562.
- [50] A. Clark, M.E. Taylor, M.J. Panzer, P. Cebe, Interactions between ionic liquid and fully zwitterionic copolymers probed using thermal analysis, Thermochim. Acta (2020), 178710.
- [51] M.E. Taylor, S.J. Lounder, A. Asatekin, M.J. Panzer, Synthesis and self-assembly of fully zwitterionic triblock copolymers, ACS Materials Letters 2 (2020) 261–265.
- [52] J. Cardoso, R. Manrique, M. Albores-Velasco, A. Huanosta, Synthesis, characterization, and thermal and dielectric properties of three different methacrylate polymers with zwitterionic pendant groups, J. Polym. Sci. B Polym. Phys. 35 (1997) 479–488.
- [53] D.J. Liaw, W.F. Lee, Thermal degradation of poly [3-dimethyl (methylmethacryloylethyl) ammonium propanesulfonate], J. Appl. Polym. Sci. 30 (1985) 4697–4706.
- [54] V.M. Boucher, D. Cangialosi, A. Alegría, J. Colmenero, Enthalpy recovery of glassy polymers: dramatic deviations from the extrapolated liquidlike behavior, Macromolecules 44 (2011) 8333–8342.
- [55] E. Lopez, S.L. Simon, Signatures of structural recovery in polystyrene by nanocalorimetry, Macromolecules 49 (2016) 2365–2374.
- [56] P. Bengani-Lutz, E. Converse, P. Cebe, A. Asatekin, Self-assembling zwitterionic copolymers as membrane selective layers with excellent fouling resistance: effect of zwitterion chemistry, ACS Appl. Mater. Interfaces 9 (2017) 20859–20872.

- [57] Y. Inoue, J. Watanabe, M. Takai, S.i. Yusa, K. Ishihara, Synthesis of sequence-controlled copolymers from extremely polar and apolar monomers by living radical polymerization and their phase-separated structures, J. Polym. Sci. Polym. Chem. 43 (2005) 6073–6083.
- [58] P.R. Bevington, D.K. Robinson, Data Reduction and Error Analysis for the Physical Sciences, 19692, McGraw-Hill, New York, 1969, pp. 235–242.
- [59] G. Szakonyi, R. Zelkó, Water content determination of superdisintegrants by means of ATR-FTIR spectroscopy, J. Pharmaceut. Biomed. Anal. 63 (2012) 106–111.
- [60] E. Hecht, Optics, fourth ed., vol. 1, Addison Wesley Longman Inc, Optics, 1998, p. 629.
- [61] F.A. Jenkins, H.E. White, D.G. Brukhard, Fundamentals of optics, AmJPh 26 (1958), 272-272.
- [62] D. Liu, C. Zhong, Modeling of the heat capacity of polymers with the variable connectivity index, Polym. J. 34 (2002) 954–961.
- [63] H. Liu, A. Uhlherr, M.K. Bannister, Quantitative structure–property relationships for composites: prediction of glass transition temperatures for epoxy resins, Polymer 45 (2004) 2051–2060.
- [64] O. Yamamuro, T. Someya, M. Kofu, T. Ueki, K. Ueno, M. Watanabe, Heat capacities and glass transitions of ion gels, J. Phys. Chem. B 116 (2012) 10935–10940.
- [65] P. Badrinarayanan, W. Zheng, Q. Li, S.L. Simon, The glass transition temperature versus the fictive temperature, J. Non-Cryst. Solids 353 (2007) 2603–2612.
- [66] C. Kittel, Introduction to Solid State Physics, Wiley, New York, 1976.
- [67] M. Pyda, X. Hu, P. Cebe, Heat capacity of silk fibroin based on the vibrational motion of poly (amino acid) s in the presence and absence of water, Macromolecules 41 (2008) 4786–4793.
- [68] Ph. D. Dissertation, Andrew Garrison Clark Fundamental Thermal Investigations of Zwitterionic Polymers, and Blends of Zwitterionic Copolymers for Targeted Energy Storage and Filtration Applications, Tufts University, Medford MA, 05/2021.